Surface Coverage Completeness for Quality-Assured Arthroscopic 3D Reconstruction

Dmitrii Bychkov, Rutwik Shah, Kaustav Mukherjee, and Mitchell So

Kaliber Labs Inc.
dmitrii@kaliberlabs.com

Abstract. 3D reconstruction from arthroscopic video is advancing rapidly, yet a fundamental question remains: how completely has the articular surface been observed? We propose a *surface coverage completeness* metric that combines raycasting-based visibility with view-quality weighting to quantify the fraction of a preoperative mesh inspected during a tracked arthroscopic session. Evaluated on 23 phantom knee sessions, binary coverage reaches $63.2 \pm 10.2\%$ of the articular envelope, but quality-weighted coverage is only $23.4 \pm 6.5\%$, revealing that much of the surface is seen only at oblique, clinically insufficient angles. We qualitatively illustrate how this quality gap correlates with TSDF reconstruction fidelity.

Keywords: Surface coverage · Arthroscopy · 3D reconstruction · Data curation

1 Introduction

3D reconstruction from endoscopic video has advanced rapidly, with methods ranging from TSDF volumetric fusion to Gaussian splatting [8], promising photorealistic spatial maps for surgical guidance. In arthroscopy, the surgeon navigates through a 4 mm endoscope with $\sim 70°$ field of view, building spatial understanding from fragmented observations. This raises a question that reconstruction alone cannot answer: *how completely has the articular surface been inspected?*

Incomplete coverage has dual consequences. *Clinically*, missed regions may harbor undiagnosed pathology—in ACL reconstruction, the intercondylar notch must be well-visualized for tunnel placement [5]. *For reconstruction*, coverage determines completeness—unobserved regions produce gaps, while obliquely-viewed regions yield degraded texture.

Related work has addressed inspection completeness in other endoscopic domains: cumulative mucosal exposure area for colonoscopy [4], topological mapping for place recognition [6], and datasets providing ground-truth geometry [2,1]. AR pipelines for arthroscopy [7] have demonstrated surface reconstruction without quantifying observation completeness. No prior work has proposed a quantitative surface coverage metric for arthroscopy or linked such a metric to 3D reconstruction quality.

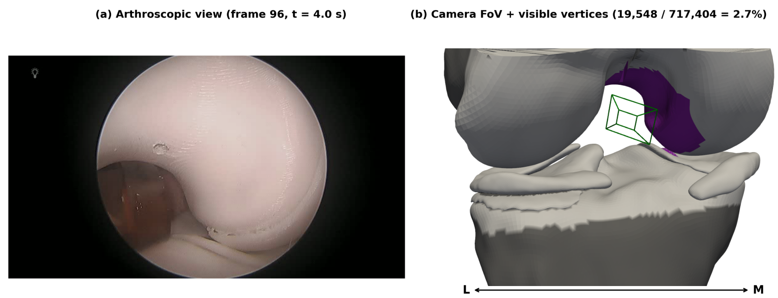

Fig. 1. Coverage computation concept. (a) Arthroscopic video frame showing a femoral condyle. **(b)** Raycasted visibility: the camera frustum (green) illuminates a region (purple) of the 3D mesh. The articular envelope is shown in light grey; non-articular bone is dark grey. Each frame's visible vertex set $\mathcal{V}_f$ is accumulated over time to compute coverage.

We present a framework combining: (1) raycasting-based visibility, (2) view-quality weighting via incidence angle, (3) an anatomically annotated articular envelope as the coverage denominator, and (4) TSDF reconstruction demonstrating how coverage quality predicts reconstruction fidelity (fig. 1).

2 Method

Visibility and Binary Coverage. Let $\mathcal{M} = \{v_i\}_{i=1}^{N}$ be the vertex set of a preoperative mesh with normals $\{\hat{n}_i\}$, and $\{(\mathbf{T}_f, \mathbf{K})\}_{f=1}^{F}$ a sequence of calibrated camera poses. For each frame f, we compute the visible vertex set $\mathcal{V}_f \subseteq \mathcal{M}$ via raycasting [9]: vertices whose triangles are hit by camera rays, are front-facing, and are not occluded. The cumulative binary coverage at frame t is:

$$C(t) = \frac{1}{|\mathcal{E}|} \left| \mathcal{E} \cap \bigcup_{f=1}^{t} \mathcal{V}_f \right| \tag{1}$$

where $\mathcal{E} \subset \mathcal{M}$ is the *articular envelope*—the set of vertices corresponding to clinically relevant cartilage surfaces (femoral condyles, tibial plateau, intercondylar region), delineated by manual annotation on the preoperative mesh.

Quality-Weighted Coverage. Binary coverage treats all observations equally, but a surface region glimpsed at a grazing angle is not equivalent to one viewed head-on. We define per-observation quality based on the incidence angle $\theta_{i,f}$ between the surface normal $\hat{n}_i$ and the viewing direction from vertex v_i toward the camera:

$$q(v_i, f) = \max\big(0,\ \cos\theta_{i,f}\big) \tag{2}$$

The quality-weighted coverage retains the best observation per vertex:

$$C_q(t) = \frac{1}{|\mathcal{E}|} \sum_{v_i \in \mathcal{E}} \max_{f \leq t} \; q(v_i, f) \tag{3}$$

The gap $C(t) - C_q(t)$ quantifies the fraction of surface seen under conditions insufficient for reliable diagnosis or reconstruction. Perpendicular viewing (θ=0) yields q=1; grazing incidence ($\theta \geq 90°$) yields q=0. *Clinically*, a lesion viewed at 70° is far harder to diagnose than at 20°; *for reconstruction*, oblique views produce elongated depth uncertainty that degrades TSDF fusion.

3 Experiments and Results

Setup. Data was acquired using an AR-guided arthroscopic navigation platform with an NDI Lyra optical tracker ($<$ 0.5 mm tracking error at 20 Hz), pre-calibrated hand-eye transformation, a 4 mm/30° arthroscope, and a 3D-printed knee phantom [3]. 23 sessions were recorded: 14 femur (7 medial, 7 lateral portal) and 9 tibia (5 medial, 4 lateral), each ∼138 s at 24 fps. Coverage was computed on a uniformly remeshed knee model (717,404 vertices; mean vertex spacing ∼0.5 mm) against a manually annotated articular envelope of 341,395 vertices (47.6% of the mesh). Vertex-based summation thus closely approximates surface area integration.

Coverage Statistics. Table 1 summarizes results by anatomy and portal (group differences evaluated via two-tailed Welch's t-tests). Overall binary coverage was 63.2 ± 10.2%; quality-weighted 23.4 ± 6.5%—a nearly 3× gap (39.8 ± 7.0 pp) revealing that much of the surface is seen only at oblique angles. Medial portals achieved higher binary coverage than lateral (66.9% vs. 59.1%; p=0.011), though quality was comparable (p=0.23). Viewing quality differed sharply by anatomy: femoral C_q=28.0% vs. tibial C_q=16.2% (p<0.001), driven by the mean incidence angle (femur 65.5° vs. tibia 83.1°; p<0.001). Quality-weighted coverage correlated strongly with mean incidence angle across sessions (r=−0.89, p<0.001).

Coverage Quality Correlates with Reconstruction Fidelity. The same tracked poses enable TSDF volumetric reconstruction via Open3D [9] (voxel size 0.25 mm; depth synthesized from poses against reference geometry). Figure 2 compares two equal-length tibia segments: the perpendicular segment ($\bar{\theta}$=52°, $\bar{q}$=0.59) yields a coherent, anatomically faithful reconstruction, while the oblique segment ($\bar{\theta}$=90°, $\bar{q}$=0.00) produces fragmented artifacts. $C_q(t)$ thus serves as a qualitative indicator of viewing geometry suitability for TSDF fusion.

Table 1. Coverage by anatomy and portal. C: binary coverage; C_q: quality-weighted coverage; Gap $= C - C_q$. Mean ± SD across sessions.

Group	n	C (%)	C_q (%)	Gap (pp)
Femur Medial	7	71.5 ± 4.5	29.2 ± 0.9	42.3 ± 4.7
Femur Lateral	7	63.0 ± 3.6	26.8 ± 0.8	36.2 ± 4.0
Femur	14	67.3 ± 5.9	28.0 ± 1.5	39.3 ± 5.2
Tibia Medial	5	60.5 ± 14.9	15.7 ± 5.3	44.8 ± 9.8
Tibia Lateral	4	52.3 ± 8.6	16.9 ± 2.5	35.4 ± 6.6
Tibia	9	56.8 ± 12.5	16.2 ± 4.1	40.6 ± 9.4
Overall	**23**	**63.2 ± 10.2**	**23.4 ± 6.5**	**39.8 ± 7.0**

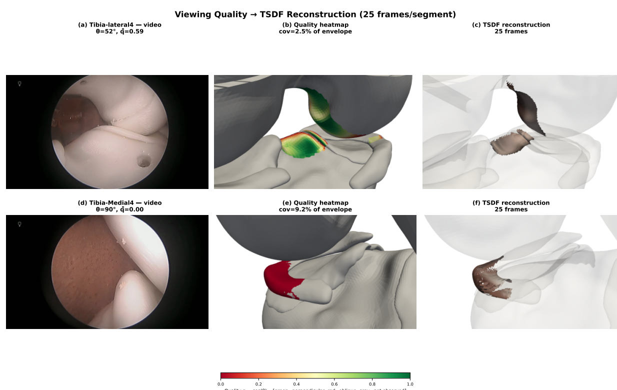

Fig. 2. Viewing quality determines reconstruction fidelity. **Top (a–c):** perpendicular viewing ($\bar{\theta}$=52°, $\bar{q}$=0.59)—quality heatmap (b) shows green vertices; TSDF fusion (c) produces a clean reconstruction. **Bottom (d–f):** oblique viewing ($\bar{\theta}$=90°, $\bar{q}$=0.00)—heatmap (e) shows red/dark vertices; reconstruction (f) is fragmented. Colorbar: $q = \cos\theta$.

4 Discussion

The nearly 3× disparity between $C(t)$ and $C_q(t)$ reveals that binary coverage alone is misleading: substantial portions of the surface are seen only at oblique angles insufficient for clinical diagnosis or faithful reconstruction. The gap $C - C_q$ identifies regions requiring re-observation.

Data Curation Implications. Lateral portals systematically under-observe medial anatomy; single-portal datasets under-represent specific regions—a bias detectable *before* model training, directly addressing the DCA-MI theme of principled data quality assessment. The quality metric further reveals that some covered regions are observed only at grazing angles, yielding images of limited value for learning-based reconstruction.

Clinical Relevance. In diagnostic arthroscopy, inspection completeness is assessed subjectively. $C(t)$ indicates whether an area was seen, while $C_q(t)$ indicates whether it was seen *well enough* to detect pathology. Integrated into AR navigation, the metric could guide surgeons to re-inspect under-observed regions during procedures.

Limitations and Future Work. This proof-of-concept evaluated 23 sessions on a single rigid phantom anatomy. Real procedures introduce tissue deformation, fluid turbidity, specular reflections, and motion blur. Portal and joint geometry also impose structural constraints. Our $q = \cos\theta$ score measures geometric viewing angle; future work will incorporate working distance, evaluate cadaveric specimens, and test coverage-guided observation planning.

References

1. Allan, M., Mcleod, J., Wang, C., Roestel, J., Kollar, P., Haase, R., Laina, I., Bano, S., Gruijia-Sola, D., Dowrick, T., Thompson, S., Clarkson, M.J., Ourselin, S., Stoyanov, D.: Stereo correspondence and reconstruction of endoscopic data challenge. In: MICCAI EndoVis Challenge (2019)
2. Bobrow, T.L., Golhar, M., Vijayan, R., Akshintala, V.S., Garcia, J.R., Durr, N.J.: C3VD: A colonoscopy 3D video dataset with paired depth from structure from motion. Medical Image Analysis **88**, 102877 (2023)
3. Erdemir, A.: Open knee(s): Virtual biomechanical representations of the knee joint. `https://simtk.org/projects/openknee` (2016)
4. Li, J., Huang, L., Luo, C., Yu, H.: Cumulative colorectal mucosal exposure area: A novel quality indicator for colonoscopy. Clinical Gastroenterology and Hepatology (2025), in press
5. Morgan, J.A., Dahm, D., Levy, B., Stuart, M.J.: Femoral tunnel malposition in ACL revision reconstruction. Journal of Knee Surgery **25**(5), 361–368 (2012)
6. Morlana, J., Tardós, J.D., Montiel, J.M.M.: ColonMapper: Topological mapping and localization for colonoscopy. In: IEEE International Conference on Robotics and Automation (ICRA). IEEE (2024)
7. Shu, H., Liu, M., Seenivasan, L., Gu, S., Ku, P.C., Knopf, J., Taylor, R., Unberath, M.: Seamless augmented reality integration in arthroscopy: A pipeline for articular reconstruction and guidance. Healthcare Technology Letters **12**(1), e12119 (2025)
8. Wang, K., Yang, C., Wang, Y., Li, S., Wang, Y., Dou, Q., Yang, X., Shen, W.: EndoGSLAM: Real-time dense reconstruction and tracking in endoscopic surgeries using Gaussian splatting. In: Medical Image Computing and Computer-Assisted Intervention (MICCAI). Springer (2024)
9. Zhou, Q.Y., Park, J., Koltun, V.: Open3D: A modern library for 3D data processing. arXiv preprint arXiv:1801.09847 (2018)